Available online at www.sciencedirect.com
ScienceDirect
Journal of Power Sources 173 (2007) 86–95
JOURNAL OF POWER SOURCES
www.elsevier.com/locate/jpowsour

Use of hydrogen–deuterium exchange for contrast in ^{1}H NMR microscopy investigations of an operating PEM fuel cell

Kirk W. Feindel, Steven H. Bergens *, Roderick E. Wasylishen [a,**]

[a] *Department of Chemistry, Gunning/Lemieux Chemistry Centre, University of Alberta, Edmonton, Alta. T6G 2G2, Canada*

Received 10 January 2007; received in revised form 30 April 2007; accepted 30 April 2007
Available online 6 May 2007

Abstract

The use of hydrogen–deuterium (H–D) exchange as a method to introduce contrast in ^{1}H NMR microscopy images and to investigate the dynamic distribution of water throughout an operating H_2/O_2 polymer electrolyte membrane fuel cell, PEMFC, is demonstrated. Cycling D_2O(l) through the flow channels of a PEMFC causes H–D exchange with water in the PEM to result in a D_2O-saturated PEM and thus concomitant removal of the ^{1}H NMR signal. Subsequent operation of the PEMFC with H_2(g) enables visualization of the redistribution of water from wet or flooded conditions as H–D exchange occurs with D_2O in the PEM and results in recovery of the ^{1}H NMR signal. Alternating between H_2(g) and D_2(g) as fuel allows observation of water distributions in the PEM while the cell is operating at a steady-state under low relative humidity. At similar currents, the rate of observable H–D exchange in the PEM during fuel cell operation was faster when the PEM was saturated with water than when under low relative humidity. These results are consistent with the known proportions of the conductive hydrophilic and nonconductive hydrophobic domains of Nafion when exposed to different relative humidities.

Keywords: Ion transport channels; In-plane water distribution; Nafion; Nuclear magnetic resonance imaging; Polymer electrolyte membrane fuel cell; H–D exchange

1. Introduction

Water management [1,2] is a key factor in commercial implementation of polymer electrolyte membrane fuel cells, PEMFCs, as alternative sources of clean, renewable energy for portable electronic devices [3], vehicles [4], and stationary power generation [5]. To achieve optimal PEMFC performance, careful design [6,7], selection of materials [8], and control of operating conditions [9] are crucial to maintain a delicate balance of water in commonly used perfluorosulfonated PEMs. For example, the protonic conductivity of Nafion is known to improve with increasing water content [10–13]; however, the accumulation of liquid water blocks catalytic sites reducing mass-transport and cell power output, and in the long term causes degradation of materials [14]. The structure of Nafion is composed of hydrophobic and hydrophilic domains, and the ion transport properties of the material are dependent on the size and distribution of the conductive hydrophilic domains. The surface area and distribution of the hydrophilic domains are dynamic, and depend on the relative humidity [15]. The hydrophilic domains occupy a larger proportion of the PEM surface, and they converge as the relative humidity is increased.

Despite the importance of water to PEMFC performance, only a few techniques are available to visualize water in situ in operating PEMFCs [16–21]. In particular, recent developments in neutron radiography methods enable quantification of the overall water content in an operating PEMFC [22–24], and advances toward visualizing water within the PEM have been reported [25]. We have demonstrated that ^{1}H NMR microscopy is an effective tool to investigate the distribution of water throughout an operating PEMFC [18], and subsequently reviewed the literature in this area [26]. Recently, using ^{1}H NMR microscopy we studied the interdependence of gas flow rates, direction of gas flow, and PEMFC power output on the in-plane distribution of water in a self-humidifying PEMFC [27]. In addition, we have reported results from ^{1}H NMR microscopy experiments which relate directly the influence of water in the PEM between the operating catalysts on the performance of a PEMFC

* Corresponding author. Tel.: +1 780 492 9703; fax: +1 780 492 8231.
** Corresponding author. Tel.: +1 780 492 4336; fax: +1 780 492 8231.
E-mail addresses: steve.bergens@ualberta.ca (S.H. Bergens), roderick.wasylishen@ualberta.ca (R.E. Wasylishen).

0378-7753/$ – see front matter © 2007 Published by Elsevier B.V.
doi:10.1016/j.jpowsour.2007.04.079

[28]. Minard et al. have also constructed a PEMFC for study via ^{1}H NMR microscopy and have reported preliminary results [20].

Previously, the use of H_2O–D_2O exchange was found to introduce contrast in ^{1}H NMR microscopy images and facilitate the study of water exchange in roots of a maize seedling [29]. Similarly, Ilvonen et al. studied water flow velocity and distribution in wood xylem [30] using H_2O–D_2O exchange. ^{1}H NMR microscopy was also used recently to investigate the mutual diffusion of H_2O and D_2O in a 3 mm diameter ball of Nafion [31]. The mechanisms and rate constants of acid and base catalyzed proton transfer in water have been thoroughly investigated via ^{1}H and ^{17}O NMR techniques [32,33].

In this study, we used hydrogen–deuterium (H–D) exchange to modify the contrast in ^{1}H NMR microscopy images of an operating PEMFC. Two methods were used to investigate the differences in utilization of the PEM ion transport channels. To investigate a PEM saturated with water, the PEM was saturated with D_2O(l) and the cell was then operated under dry H_2(g). To investigate a PEM at low relative humidity, the cell was operated for a period of time under dry D_2(g), and then the fuel switched to H_2(g), or vice versa. Recovery or loss of the ^{1}H NMR signal was monitored, as required (vide infra).

2. Experimental

A representation of the disassembled PEMFC used for this investigation is shown in Fig. 1. The gas inlets/outlets are at the top of the cell. The planes of the membrane electrode assembly, MEA, and the gas flow channels are oriented parallel with the direction of the static applied magnetic field, B_0. The MEA was constructed using a hot-press decal-transfer method [34] with unsupported HiSpec 1000 Pt black and HiSpec 6000 Pt–Ru black for the cathode and anode catalyst (loadings ~2–3 mg cm^{-2}), respectively. The geometric area of each catalyst decal is ~0.5 cm^2. Nafion-117 was used as the PEM and Toray TGP-H-060 carbon paper as the gas diffusion layer, GDL, and current collector. Further details regarding the design and construction of the PEMFC are given elsewhere [18,26,27].

Pre-purified H_2(g) (99.995%) or D_2(g) (99.70%) and industrial grade O_2(g) (99.0%) were supplied at ambient pressure to the PEMFC from compressed gas cylinders via flow meters. All gases were obtained from Praxair. D_2O(l) (99.9%) was obtained

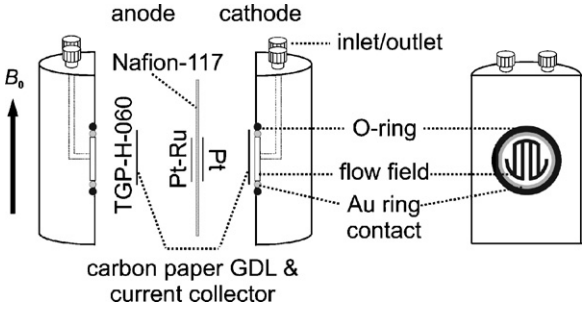

Fig. 1. Assembly schematic of the PEMFC indicating the components and their location and the orientation of the PEMFC with respect to the applied magnetic field B_0.

from Cambridge Isotopes or General Intermediates of Canada. Dry gases were used, and unless otherwise stated, the H_2(g) or D_2(g) flow rate was 5 mL min^{-1} and the O_2(g) flow rate was 2.5 mL min^{-1}. For this study the PEMFC was operated at external resistances that, in the absence of flooding of the catalysts by water, resulted in power densities ranging from approximately 15–50 mW cm^{-2}. In addition, the effective stoichiometry varied from ~15–60 for both the anode and the cathode gas flows. Prior to cycling D_2O(l) through either the cathode or anode with a systolic pump, H_2O(l) accumulated in the cathode flow channels was purged using an O_2(g) flow rate of 50 mL min^{-1}. A flow of N_2(g) (99.93%) was used to remove most H_2(g) from the anode gas lines and flow channels before D_2O(l) was cycled through the anode flow channels.

^{1}H NMR microscopy experiments were performed using a 7.05 T vertical wide bore superconducting magnet, Bruker Avance 300 console, Micro-2.5 imaging accessory, and 30 mm inner diameter birdcage resonator. The water-cooled gradient unit was maintained at 20 °C, and this is assumed to be the operating temperature of the PEMFC. A slice-selective spin–echo imaging sequence [35] was used to obtain images from a 30 mm × 30 mm field of view. Five slices of thickness 500 μm were oriented such that the entire PEM and most of each GDL were contained within the central slice and the anode and cathode flow fields contained in the neighboring slices. The frequency encode direction was parallel with the plane of the MEA and B_0. 128 frequency and 128 phase encode steps were used, yielding an in-plane pixel size of 234 μm × 234 μm. This resolution is similar to that obtainable from neutron radiography with available scintillator and detector combinations [25]. In all experiments, the time between ^{1}H NMR signal excitation and acquisition of the first echo, T_E, was 3.2 ms, and in total eight echoes were co-added after each excitation. The length of the RF excitation pulse was 1.0 ms with a BW of 6 kHz and a flip angle, α, of 90°. In all experiments, the receiver BW was 101010.1 Hz, the repeat time between successive ^{1}H NMR signal excitations, T_R, was 1.0 s, resulting in a total time of 128 s for each image. For water in acid-form Nafion, the ^{1}H NMR spin–lattice relaxation time, T_1, has been reported over a range of water contents [12,36]. In general, the PEM in an operating PEMFC is not fully hydrated and therefore T_R = 1.0 s is sufficiently long to prevent significant saturation of the ^{1}H NMR signal from H_2O in the PEM. As well, the presence of paramagnetic components in the MEA (e.g., catalysts, O_2(g)) reduces the ^{1}H T_1 values [37].

3. Results and discussion

Fig. 2a shows an example of the orientation of a slice through the PEMFC selected for ^{1}H NMR microscopy. The total thickness of the MEA is ~580 μm, assuming that Nafion-117 swells to a thickness of ~200 μm [38,39] and each GDL is 190 μm thick. Therefore, images are typically collected from a series of five slices, each 500 μm in thickness; most of the MEA is contained in a single slice and the bordering slices contain the flow fields [26,27]. Images acquired from a slice containing the MEA, and a flow field filled with H_2O(l), are shown in Figs. 2b and c, respectively. Fig. 2d is a photograph of the O-ring, Au

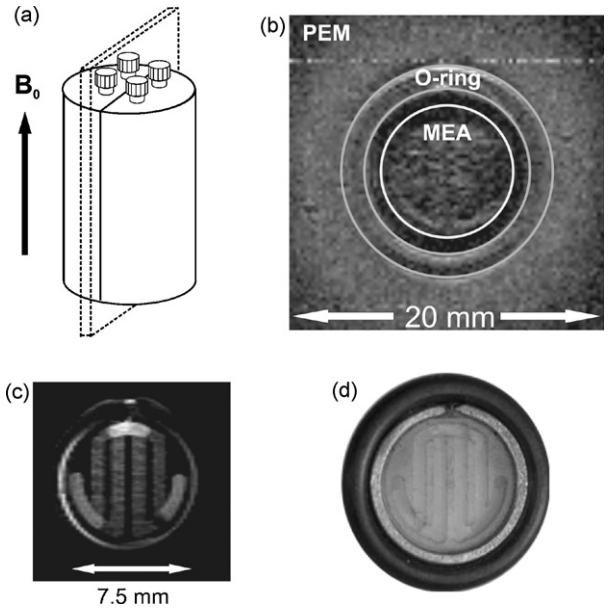

Fig. 2. (a) Schematic of the assembled PEMFC and the orientation of a slice selected for NMR microscopy, (b) ^{1}H NMR microscopy image from a 500 μm slice containing the MEA; the location of respective components are labeled, (c) ^{1}H NMR microscopy image from a 750 μm slice containing a flow field filled with H_2O(l), and (d) a photograph of the O-ring, Au ring, and flow field.

ring, and flow field of one half-of the PEMFC and shows the location of the components relative to the ^{1}H NMR microscopy images.

3.1. Contrast introduced via H–D exchange between protons the PEM and D_2O(l)

Fig. 3a depicts a configuration of the gas inlets/outlets. Fig. 3b indicates the direction of gas flow in the anode and cathode flow fields for this counter-flow configuration from the perspective of the images herein, i.e., viewed from the anode side of the PEMFC. Fig. 4a shows a ^{1}H NMR microscopy image from a 500 μm thick slice containing the MEA, acquired after operating the PEMFC on dry H_2(g) and dry O_2(g) for ~4 h at ~14 mW cm^{-2} (11 mA, 0.63 V, electrode area ~0.5 cm^2). This image represents a steady-state amount and distribution of water in the PEM determined by the gas flow and the water produced from the reduction of oxygen at the cathode. At $t = 0$ the circuit with the external resistance was disconnected (i.e., $I = 0$ mA), the H_2(g) and O_2(g) flows were stopped, and D_2O(l) was pumped into the cathode flow field. The images in Fig. 4b–d show the

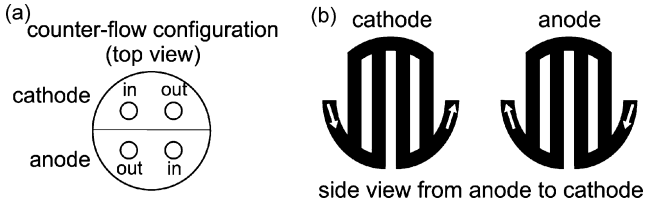

Fig. 3. (a) Schematic of the top of the PEMFC showing the gas inlets/outlets in a counter-flow configuration, (b) the direction of gas flow through the cathode and anode flow channels as viewed from the anode side of the PEMFC.

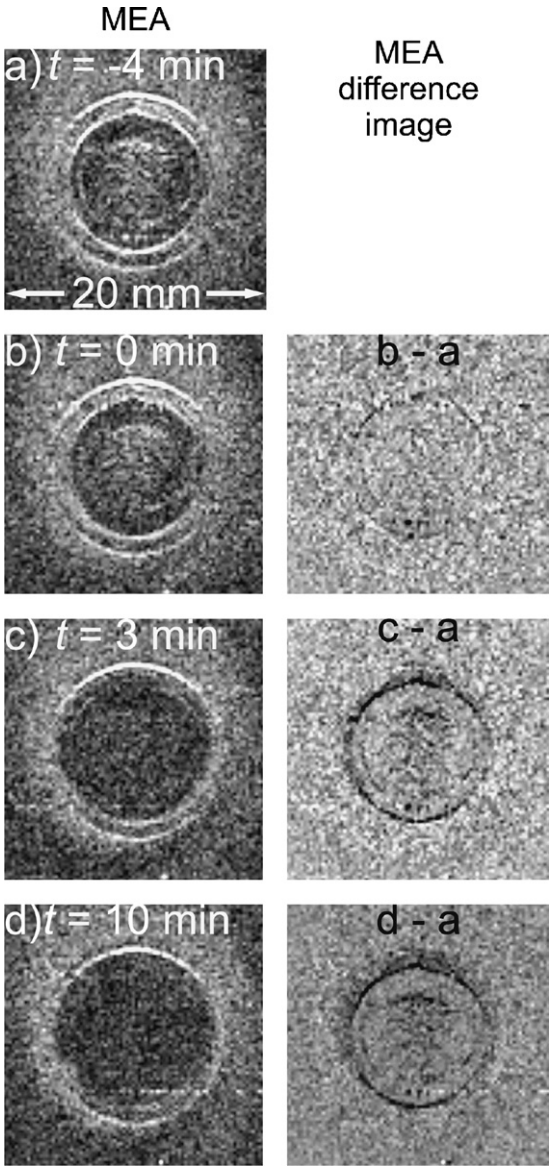

Fig. 4. ^{1}H NMR microscopy images from a 500 μm slice containing the MEA (left) and MEA difference images (right) acquired from the PEMFC (a) operating on dry H_2(g) and O_2(g) 4 min prior to pumping D_2O(l) into the cell, (b) and (c) when D_2O(l) was cycled through the cathode flow field starting a $t = 0$, and (d) after the D_2O(l) was purged from the PEMFC with O_2(g). The MEA difference images show the decline in ^{1}H NMR signal.

decline of the ^{1}H NMR signal as H–D exchange occurs between the D_2O(l) passed through the cathode flow field and the protons in the PEM. Decreases in image intensity due to exchange with D_2O only occur in areas of the PEM that contain H_2O, i.e., a dry PEM will not exhibit change in ^{1}H NMR signal upon hydration with D_2O. Each MEA difference image shows the loss of ^{1}H NMR signal relative to the image in Fig. 4a. The ^{1}H NMR signal decreased rapidly in the MEA region, such that by $t = 3$ min there was little signal remaining. When no further reduction in the ^{1}H NMR signal from the MEA region was noticeable, the D_2O(l) was purged from the cathode flow channels with O_2(g) at a flow rate of 50 mL min^{-1} and the image in Fig. 4d was acquired. Often, after cycling H_2O(l) or D_2O(l) through the flow channels

only a low power output was attainable (e.g., <5 mW cm^{-2}). The expected performance was not achieved until high gas flow rates of 25–50 mL min^{-1} were used to remove excess liquid water from the GDL and catalysts. After being in contact with D_2O(l) the PEM is expected to be completely hydrated and the conductive hydrophilic domains of the PEM swollen to a maximum to facilitate efficient ion transport [40,41].

Shown in Fig. 5a is an image acquired after purging the D_2O(l) from the cathode flow channels and 3 min prior to initiating the H_2(g) flow or drawing a current from the PEMFC. This image represents high water (D_2O) content, but low ^{1}H density in the MEA. At $t = 0$ the H_2(g) and O_2(g) flow rates were set to 5.0 and 2.5 mL min^{-1}, respectively. The external resistive circuit was reconnected and the PEMFC power output adjusted to ~25 mW cm^{-2} (19.5 mA, 0.623 V). After operating the cell for 10 min (Fig. 5b) at ~25 mW cm^{-2}, the onset of recovery of the ^{1}H NMR signal in the MEA region (i.e., inside the O-rings) is evident in both the image from a slice containing the MEA and the difference image. The ^{1}H NMR signal continued to intensify, and after operating for ~90 min (Fig. 5d) there was a relatively uniform distribution of water in the PEM of the MEA. Also, water was evident along the Au ring. The difference images in Fig. 5b–d reveal a faint ring-shaped region beyond the MEA. This darker region indicates that D_2O was transported from the MEA region into the surrounding PEM. Radial diffusion outward from the MEA was also observed during fuel cell startup with a dry membrane [18].

As shown by the images in Fig. 5, the region of the PEM between the operating catalyst layers, i.e., the MEA (see Fig. 2b), quickly reflects an increase in ^{1}H NMR signal intensity as H–D exchange occurs between the D_2O in the PEM and the H_2(g) oxidized at the anode. The ^{1}H NMR signal intensity (in arbitrary units) in the MEA region (904 pixels, 0.497 cm^2) was integrated, and a plot of the values versus the time that the PEMFC operated on H_2(g) as fuel is shown below the images in Fig. 5. Note that for the first ~60 min, on average, the integrated intensity values steadily increased and then plateaued. These observations indicate that the H–D exchange in the MEA region of the PEM began immediately upon operating the PEMFC with H_2(g) and was essentially complete after ~60 min. Such a rapid onset of the increase in ^{1}H NMR signal is expected when a large proportion of the D_2O-saturated ion transport channels in the Nafion are involved in proton conduction. The minor fluctuations observed in the values of the integrated intensity result from interference artifacts in the images which can typically be removed by signal averaging, albeit with increased experimental time.

To account for the observations presented thus far, several exchange and transport phenomena are considered. Flowing H_2(g) through the anode flow channels without drawing a current from the PEMFC may lead to H–D exchange with water in the PEM at the catalyst surface:

$$\text{Pt–H} + D_2O \leftrightarrow \text{Pt–D} + \text{HDO} \quad (1)$$

When the PEMFC is not operated the transport of water to and from the catalyst is limited by the self-diffusion rate of water in the PEM. H–D exchange in the D_2O-saturated PEM is facilitated

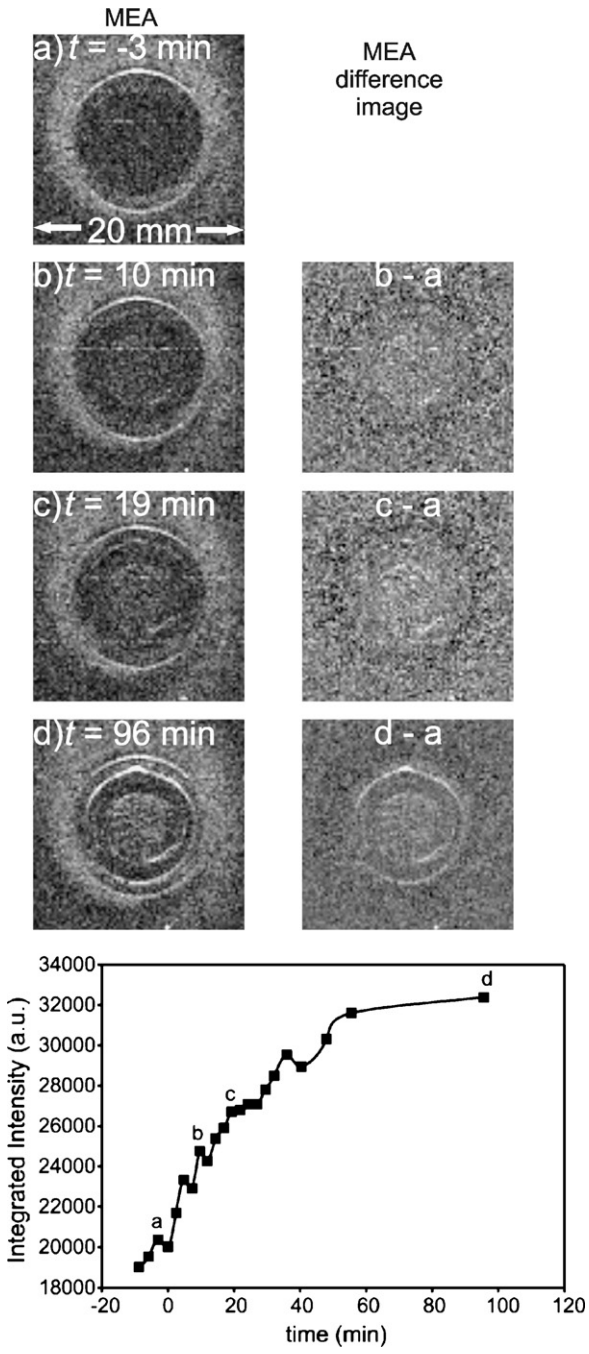

Fig. 5. ^{1}H NMR microscopy images from a 500 μm slice containing the MEA (left) and MEA difference images (right) acquired from the PEMFC (a) after purging D_2O(l) from the cathode flow field with O_2(g), and (b)–(d) after operating on dry H_2(g) and O_2(g) for the indicated time. $t = 0$ was when the H_2(g) flow was started and current was drawn from the PEMFC. The MEA difference images show the increase in ^{1}H NMR signal as H–D exchange occurred with D_2O in the PEM upon operating the cell with H_2(g) as fuel and a faint dark ring from D_2O diffusing away from the MEA. The plot shows the integrated ^{1}H NMR signal intensity in the MEA region (see Fig. 2b) vs. PEMFC operating time.

by operating the PEMFC since H_2(g) is oxidized at the anode and protons are transported through the PEM to the cathode. For a current of 20 mA the rate of proton consumption at the cathode is ~2.1×10^{-7} mol s^{-1}. Two reactions describe the H–D exchange

process with D_2O in the PEM:

$$D_2O + H^+ \leftrightarrow HOD + D^+$$
$$HOD + H^+ \leftrightarrow H_2O + D^+ \quad (2)$$

The rate constant for proton exchange in pure H_2O(l) at 28 °C is $7.1 \pm 0.4 \times 10^9$ L mol^{-1} s^{-1} and for deuteron exchange in D_2O(l) is $4.3 \pm 0.5 \times 10^9$ L mol^{-1} s^{-1} [42]. The mean lifetime of a water molecule in solution before proton exchange is related to pH (in this case pD), and for acidic environments the mean lifetime (in seconds) can be approximated by the relation $10^{pH-9.85}$ [42]. Acid-form Nafion is a very strong Brønsted acid, with strength comparable to that of CF_3SO_3H [43]. Thus, H–D exchange in water saturated Nafion is fast on the NMR chemical shift timescale (i.e., <μs).

Water transport in the PEM can occur via self-diffusion, Fickian or concentration-dependant diffusion, pressure gradients [44], and in an operating PEMFC via electro-osmotic drag [2,45]. After cycling D_2O(l) through the flow channels, the MEA is expected to be fully hydrated, i.e., the size of conductive hydrophilic domains are at a maximum; however, changes in PEM water content outside of the MEA, beyond the O-rings occur more slowly than within the MEA. The PEM surrounding the MEA is thereby not saturated with water during these experiments. Thus, the diffusion of D_2O outward from the MEA may occur via a combination of mechanisms. Grotthus hopping is not expected to distribute D^+ more rapidly than the rate of self-diffusion. The diffusion coefficient for H_2O in Nafion-117 (~36 wt.%, $n H_2O/SO_3H = \lambda = 22$) at 298 K is $\sim 7.4 \times 10^{-10}$ m^2 s^{-1} [45]. A preliminary ^{1}H NMR microscopy investigation of a 3 mm diameter ball of Nafion saturated with H_2O and subsequently placed in D_2O(l) determined a H_2O–D_2O mutual diffusion coefficient of 2.5×10^{-10} m^2 s^{-1} [31]. For comparison, at 298 K the self-diffusion coefficients of H_2O(l), 50 mol% H_2O–D_2O(l), and D_2O(l) are $23.0 \pm 0.2 \times 10^{-10}$ m^2 s^{-1} [46], $20.29 \pm 0.04 \times 10^{-10}$ m^2 s^{-1}, and $18.72 \pm 0.04 \times 10^{-10}$ m^2 s^{-1} [47,48], respectively. Assuming that the diffusion coefficients of D_2O and H_2O in Nafion-117 scale as for the pure liquids, an estimation of the upper limit for the diffusion coefficient of D_2O in Nafion-117 is $\sim 6 \times 10^{-10}$ m^2 s^{-1}. The mean square displacement, $\langle r^2 \rangle$, of a particle with a translational diffusion coefficient, D, after a time, t, can be treated as a random walk process [49], where in one dimension $\langle r^2 \rangle = 2Dt$. Thus, the maximum linear displacement, r, of D_2O in Nafion-117 due to translation diffusion after 60 min is ~2.1 mm. The time required for H–D exchange to occur in the PEM beyond the region in contact with D_2O(l) (i.e., outside the O-rings) depends on both the translational diffusion of water in the PEM and the volume of the PEM outside the O-rings. The dark ring observed in the MEA difference image shown in Fig. 5d extends approximately 7 mm beyond the O-rings ~100 min after D_2O(l) was cycled through the cathode flow field and the cell was subsequently operated with H_2(g) as fuel. This distance is greater than expected from only translational self-diffusion and implies that the effective rate of translational diffusion is increased either by ionic conduction or a water concentration gradient between the area within and outside the O-rings.

3.1.1. Influence of gas inlet/outlet configuration on the distribution of water in the PEM between the operating catalyst layers

A summary of the influence of operating the PEMFC under counter- and co-flow gas configurations when using D_2O(l) to introduce exchange-contrast is shown in Fig. 6. The images shown in Fig. 6a and b were obtained when the cell was first operated with dry H_2(g) and O_2(g) in counter-flow configurations. Our previous experiments show that this mode of operation results in a more uniform in-plane distribution of water in the PEM between the operating catalyst layers than when the gases

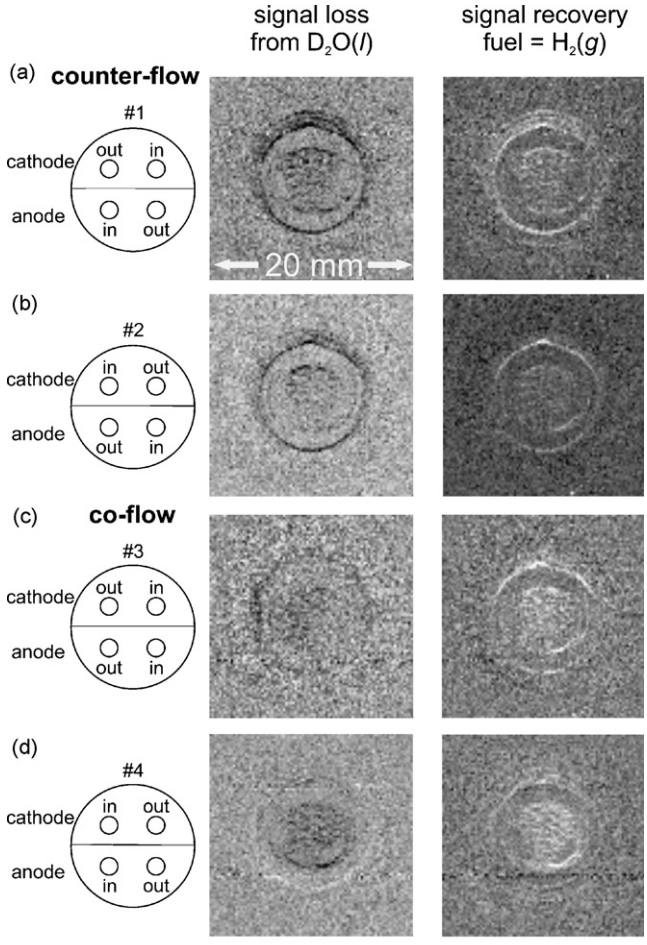

	Operating time	Power / mW cm^{-2}
	signal recovery	
a)	1324 min	~32 to 30
b)	99 min	~25
c)	55 min	~9 to 35
d)	89 min	~4 to 31

Fig. 6. Schematic of the top of the PEMFC indicating the gas inlet/outlet configurations (left), MEA difference images showing the decline in ^{1}H NMR signal in the PEM caused by cycling D_2O(l) through either the cathode or anode flow field (centre), and MEA difference images showing the increase in ^{1}H NMR signal in the PEM upon operating the PEMFC on dry H_2(g) as fuel (right). The table shows the period of time that the PEMFC operated on H_2(g) at the indicated power prior to acquiring the image of the MEA used in the calculation of the signal recovery image.

are in a co-flow configuration [27]. Indeed, subsequent introduction of D_2O(l) results in dark regions in the signal loss images that are relatively uniform across the plane of the PEM, showing where H–D exchange occurs between water in the PEM and D_2O. The H–D exchange that occurs when the PEMFC is subsequently operated with H_2(g) as fuel is shown in the signal recovery images. As expected for a fully hydrated PEM, the ^{1}H NMR signal recovery is uniform in the plane of the MEA.

For co-flow configuration #3 (Fig. 6c), prior to cycling D_2O(l) through the cathode, the cell was operated for ∼20 h with a power output of ∼30 mW cm^{-2} and had not been flooded with H_2O(l) or D_2O(l) for several days. Therefore, the content and distribution of water in the PEM was determined by the operating conditions (e.g., gas flows, power output) of the cell. Upon cycling D_2O(l) through the cathode, the loss of the ^{1}H NMR signal occurred predominantly at the gas outlets and indicates that the water content of the PEM was high near the gas outlets and low near the gas inlets, as expected for a co-flow gas configuration [27]. In contrast, for the co-flow configuration #4, D_2O(l) was cycled through the cathode flow channels immediately prior to operating the PEMFC at ∼4 to 31 mW cm^{-2} for 90 min. As shown by the images in Fig. 6d, the loss of ^{1}H NMR signal intensity was more uniform across the MEA in comparison to that observed for configuration #3. This indicates that the PEM water content resulting from cycling the D_2O(l) through the flow channels was sufficiently high to compensate for water removed by the dry gases entering the flow channels during operation of the PEMFC over the 90 min period. The uniform distribution of water observed for configuration #4 also indicates that the amount of water in the PEM had not reached a steady-state after operating the cell for 90 min, as the region of the PEM near the gas inlets would typically be dehydrated [27].

Saturating the MEA with D_2O(l) and then operating the PEMFC with H_2(g) as fuel results in H–D exchange with water in the PEM. The signal recovery images in Fig. 6 reveal that, as expected, the exchange occurs uniformly across the plane of the MEA for all gas flow configurations.

3.2. Contrast introduced by alternating between H_2(g) and D_2(g) as fuel: H–D exchange under low relative humidity

We have shown that changes in the in-plane distribution of water in the MEA of an operating PEMFC can be observed by ^{1}H NMR microscopy [18,27], and by using D_2O(l) to introduce image contrast in water-saturated PEMs (Section 3.1). Due to the relatively constant content and distribution of water in the PEM of a fuel cell operating at steady state, investigating minor variations of water within the PEM is difficult. Here we demonstrate that contrast can be introduced into the ^{1}H NMR microscopy images of an operating PEMFC by alternately fuelling the PEMFC with H_2(g) and D_2(g). We also demonstrate that such experiments give an indication of the proportion of ion transport channels utilized by the membrane.

A ^{1}H NMR microscopy image acquired after the PEMFC operated on H_2(g) and O_2(g) in counter-flow configuration #1 (see Fig. 6a) with a power output of ∼30 mW cm^{-2} for 7 h is shown in Fig. 7a. The images show that the PEM was hydrated and that a small amount of H_2O(l) was in the cathode flow field. At $t = 0$ the external circuit was disconnected (i.e., $I = 0$ mA) and the fuel was switched from H_2(g) to D_2(g). When the circuit was reconnected, the cell power output was the same as measured when using H_2(g) as fuel. For a Pt catalyst at 25 °C, and 1 atm, the exchange current densities for the anode and cathode of an H_2/O_2 PEMFC are ∼10^{-4} and ∼10^{-9} A cm^{-2}, respectively [50]. In theory, the open circuit voltage of a D_2/O_2 PEMFC should be marginally higher than for a H_2/O_2 PEMFC since the Gibbs' free energy of formation for D_2O(l) is ∼5 kJ mol^{-1} larger than for H_2O(l). There are reports of a fourfold decrease in power output when using a low partial pressure (0.7 kPa) of D_2(g) versus H_2(g) [51,52]. This effect was attributed to proton-tunneling between adjacent sulfonate groups at the surface of the PEM and becomes less important with increasing partial pressure of D_2(g) [51,52]. More investigations are required to determine the origin of deuterium isotope effects on the performance of PEMFCs.

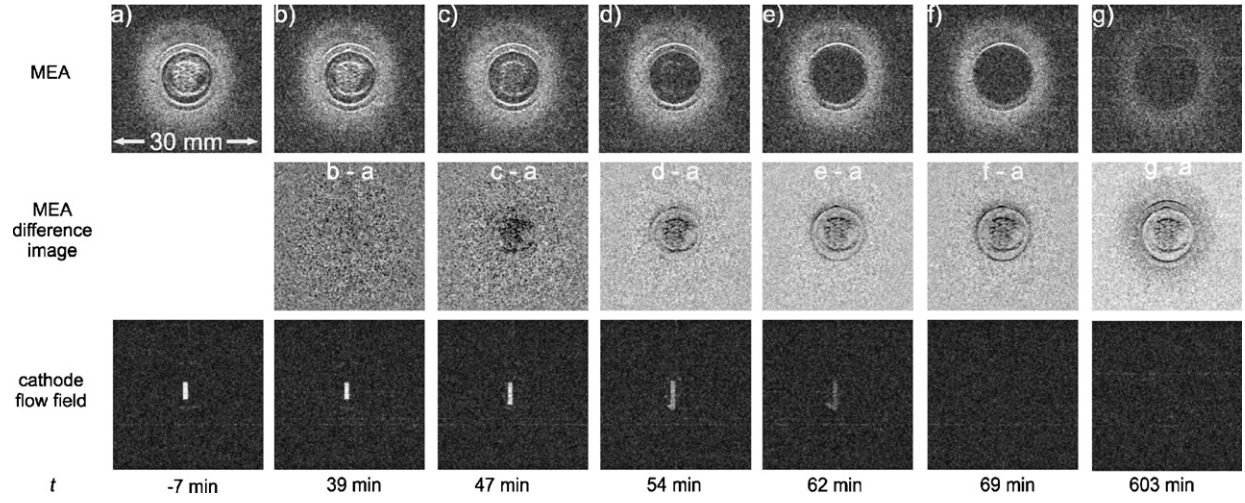

Fig. 7. ^{1}H NMR microscopy images from 500 μm slices containing the MEA (top), the cathode flow field (bottom), and the MEA difference images (middle) showing the decrease in ^{1}H NMR signal while operating the PEMFC on D_2(g) as fuel with a power output of ∼30 mW cm^{-2} (22 mA, 0.67 V). At $t = 0$, the fuel was switched from H_2(g) to D_2(g).

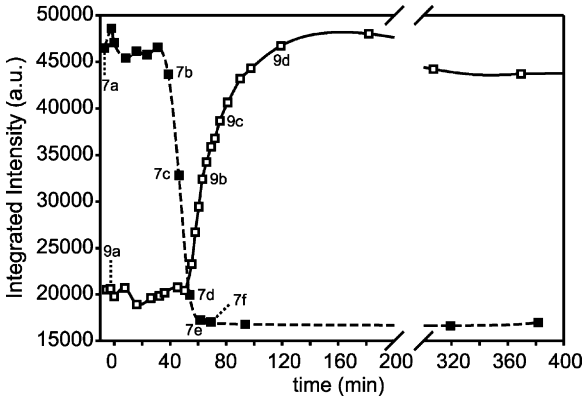

Fig. 8. Plots of the integrated ^{1}H NMR signal intensity from the MEA region (see Fig. 2b) vs. PEMFC operating time, corresponding to the datasets shown in Fig. 7 (■) and Fig. 9 (□).

The difference image (see Fig. 7b) and the corresponding integrated signal intensity from the MEA region (see Fig. 8, ■) show that the ^{1}H NMR signal in the MEA only started to decline after using D_2(g) as fuel for 39 min, in stark contrast to the experiments in which the PEM was saturated with water first, when the signal started to decline within 10 min. The amount of water observed in the cathode flow field increased as the H–D exchange became more apparent (Fig. 7c–e). After 69 min little ^{1}H NMR signal remained in the MEA or in the flow field. Although the water that had accumulated in the cathode flow field was no longer visible in the images, no unusual fluctuations in power output were observed that would suggest removal of the water from the flow field [27]. After operating the PEMFC with D_2(g) for a period of 600 min a significant decline of the ^{1}H NMR signal was evident outside of the MEA in the surrounding PEM (Fig. 7g).

When operating with D_2(g) as fuel, no significant loss of the ^{1}H NMR signal in the MEA (as shown by the plot in Fig. 8, ■) or cathode flow field occured during the first 40 min. Operating the PEMFC with a current of 23.5 mA uses approximately 1.22×10^{-7} mol s^{-1} of D_2(g) and produces the same amount of water at the cathode. As shown in the images in Fig. 7b, the 2.9×10^{-4} mol of D_2(g) consumed and the ~5.3 μL of water produced over the first 40 min do not affect the ^{1}H NMR signal in the MEA. This volume of water produced, however, should be sufficient to fully exchange the existing water contained in the PEM between the operating catalyst layers if all of the ion transport channels are involved in proton/deuteron conduction. The ^{1}H NMR signal starts to observably decline in the membrane only after the first 40 min. Exchange within the MEA and with the water accumulated in the cathode flow field appears complete after 30 min of further operation.

The images in Fig. 9 show the recovery of the ^{1}H NMR signal due to H–D exchange after the fuel was switched from D_2(g) to H_2(g). Prior to acquiring the images in Fig. 9a the PEMFC was operated using D_2(g) as fuel with a power output of ~30 mW cm^{-2} (23.5 mA, 0.70 V) for ~3 h in counter-flow configuration #1 (see Fig. 6a). Only after approximately 60 min of operating with H_2(g) as fuel and a power output of ~30 mW cm^{-2} did the ^{1}H NMR signal in the MEA and the

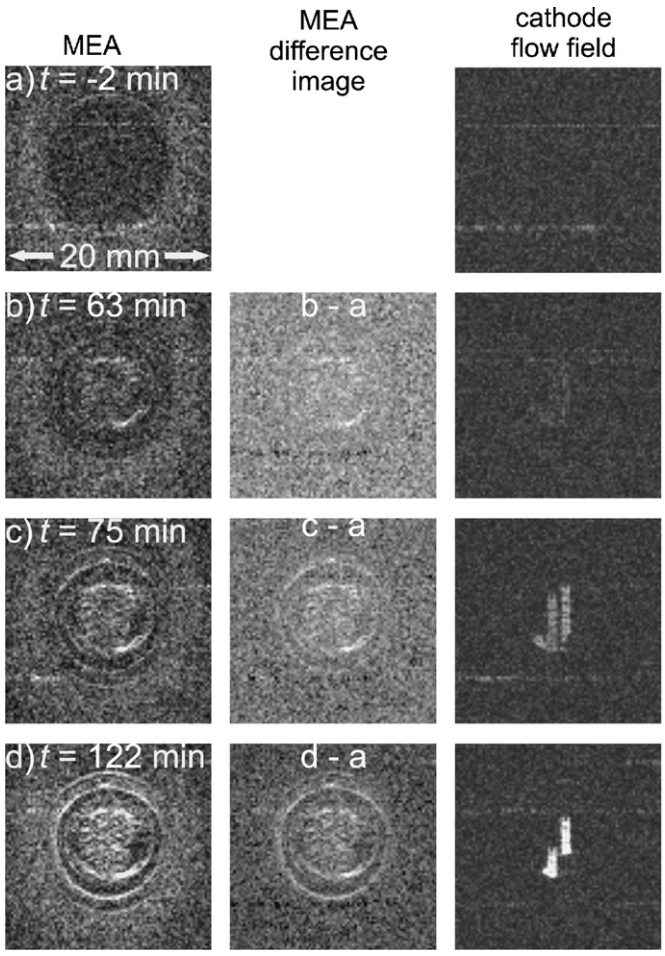

Fig. 9. ^{1}H NMR microscopy images from 500 μm slices containing the MEA (left), the cathode flow field (right), and the MEA difference images (centre) showing the increase in ^{1}H NMR signal while operating the PEMFC on H_2(g) as fuel with a power output of ~30 mW (23 mA, 0.65 V). At $t = 0$, the fuel was switched from D_2(g) to H_2(g).

cathode flow field become evident (Fig. 9b). The corresponding plot of the integrated ^{1}H NMR signal intensity values from the MEA region of the image versus time see Fig. 8, □) shows that the increase in the integrated intensity begins shortly before $t = 60$ min. The intensity of the ^{1}H NMR signal continued to increase over a period of 120 min, apparent from the images in Fig. 9c and d and the plot in Fig. 8.

Several exchange and transport processes may contribute to these observations. In addition to the exchange processes discussed in Section 3.1 for H–D exchange with water in the PEM, exchange will also occur between the gases at the catalyst surface:

$$2\,(\text{Pt–H}) + D_2 \leftrightarrow 2\,(\text{Pt–D}) + H_2 \quad (3)$$

Upon electro-oxidation of the fuel, H–D exchange will occur with water in the PEM to form HOD and eventually D_2O or H_2O. As H–D exchange occurs, water in the PEM may diffuse away from the MEA due to a concentration gradient, be transported via intradiffusion or through the PEM to the cathode via electro-osmotic drag. Each of these processes will increase the volume over which H–D exchange occurs. In addition, if water

is accumulated in the cathode flow field, back-diffusion will increase the total volume of water to be exchanged. In theory, if the rates of the water transport processes were known, the amount of water contained in the PEM could be calculated from the rate of fuel consumption and the period of time required for complete exchange to occur.

When operating on D_2(g), the decline in signal was apparent after 40 min (Fig. 7b, Fig. 8, ■), whereas when operating on H_2(g) the recovery of the signal was not apparent for almost 60 min (Fig. 9b, Fig. 8, □). These observations were reproducible over repeated experiments; the time required for an apparent change in image intensity, for signal decline over seven separate experiments, ranged from 33 to 45 min with an average time of 39 min, and for signal recovery over six separate experiments, ranged from 58 to 77 min with an average of time 64 min. The rate of H–D exchange with water in the PEM is related to the hydrating species. The deuteron exchange rate for D_2O is slower than the proton exchange rate for H_2O; therefore, one might expect the recovery of the ^{1}H NMR signal in a D_2O-containing PEM to take longer than the signal decline in a H_2O-containing PEM when operating the PEMFC on H_2(g) and D_2(g), respectively. While this is consistent with our observations, a more detailed explanation may be necessary for this complex system.

3.2.1. Time required for H–D exchange: PEM saturated with water versus low relative humidity

After the PEM was saturated with D_2O and the PEMFC was operated with H_2(g) as fuel, the integrated ^{1}H NMR signal intensity values from the MEA region immediately began to increase (see Fig. 5). In contrast, when the fuel was switched from H_2(g) to D_2(g), or vice versa, there was a significant delay before changes in the ^{1}H NMR signal were observed, despite that more water was generated electrochemically by the cell than was present in the membrane between the catalyst layers. The primary difference in experimental conditions between the two H–D exchange methods is that the PEM is saturated with water in the H_2(g)/D_2O(l) method, whereas the H_2(g)/D_2(g) method results in a low relative humidity environment. The water uptake of Nafion is known to depend on whether the PEM is in contact with water vapor or liquid water [11,38,45]. This difference is commonly referred to as Schroeder's paradox [53] and is thought to result from the hydrophobic fluorine-rich surface morphology of Nafion [41,54]. Atomic force microscopy, AFM, techniques have been used to investigate the hydrophilic and hydrophobic regions of Nafion at various levels of hydration [40,41]. Clusters of hydrophilic domains of 4–10 nm in diameter at ambient humidity were found to swell to 7–15 nm in diameter when the Nafion was in contact with liquid water [41], and clusters up to 40 nm in width have been reported [55]. The number of clusters was found to decrease as the cluster size increased [40]; however, the overall area of the Nafion surface covered by the conductive hydrophilic domains increases with greater relative humidity [55]. The increased size of the hydrophilic clusters significantly improves the ion transport properties of Nafion [55]. In the ^{1}H NMR microscopy experiments, the onset of observed H–D exchange began sooner over a large portion of the PEM between the catalyst layers when the PEM was saturated with D_2O (∼10 min) than when operating under low relative humidity (40–60 min), despite that in both cases the total ionic current passing through the membrane was similar (∼20 mA versus 22 mA). We therefore propose that a smaller volume of the hydrophilic domains

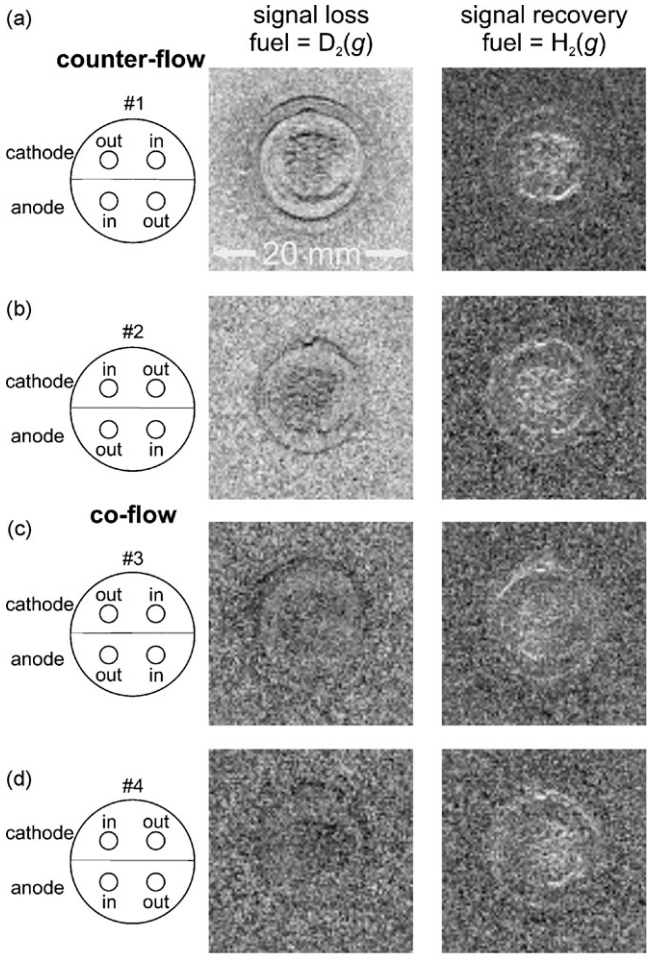

	Operating time	Power / mW cm^{-2}
	signal loss	
a)	603 min	~32 to 30
b)	67 min	~32
c)	123 min	~25 to 31
d)	83 min	~25 to 30
	signal recovery	
a)	83 min	~32 to 30
b)	104 min	~34 to 32
c)	92 min	~32 to 29
d)	86 min	~31 to 29

Fig. 10. Schematic of the top of the PEMFC indicating the gas inlet/outlet configurations (left), MEA difference images showing the decline in the ^{1}H NMR signal in the PEM when using D_2(g) as fuel (centre), and MEA difference images showing the subsequent increase in the ^{1}H NMR signal when using H_2(g) as fuel (right). The table shows the period of time that the PEMFC operated on D_2(g) (signal loss) or H_2(g) (signal recovery) at the indicated power prior to acquiring the final image of the MEA used in the calculation of each MEA difference image.

are involved in ion transport and that the current per conductive area is higher when the PEM is operated at low relative humidity than when it is saturated with water.

3.2.2. Influence of gas inlet/outlet configuration on distribution of water

The influence of co- and counter-flow gas configurations on the exchange-contrast introduced in the ^{1}H NMR microscopy images of the PEM by alternating between D_2(g) and H_2(g) as fuel was also investigated. In Fig. 10 two MEA difference images are shown for each configuration. The first image shows the decline of the ^{1}H NMR signal when the fuel is switched from H_2(g) to D_2(g), and the second image shows the recovery of the signal when H_2(g) was subsequently used as fuel. In the counter-flow configurations, #1 and #2, the H–D exchange in the PEM was relatively uniform in the plane of the MEA. This indicates a uniform in-plane distribution of water in the PEM and facilitates effective use of most of the catalyst decal. The images in Fig. 10c and d show the non-uniform in-plane distribution of water in the PEM that results when the cell operates in the co-flow configurations. In both co-flow configurations there is little variation in the image contrast in the region near the gas inlets, indicating that the PEM in this region contains little water. As a result, the conductivity of the PEM varies across the plane of the MEA from gas inlet to outlet. In addition, only the region of the catalyst stamp near the gas outlets, where the water content and proton conductivity are higher, is used effectively. The variation in the distribution of water in the PEM for the co-flow versus counter-flow gas configurations observed using H–D exchange is consistent with the results reported when starting the PEMFC with low water content PEM [27].

4. Conclusions

The results presented here demonstrate that H–D exchange can be used effectively to introduce contrast related to water distribution in ^{1}H NMR microscopy images of an operating PEMFC. After operating the PEMFC on H_2(g), cycling D_2O(l) through the cathode or anode flow channels rapidly removed the ^{1}H NMR signal within the MEA and revealed where H_2O was contained in the PEM. Subsequent operation of the PEMFC with H_2(g) as fuel facilitated the investigation of changes in water content when operating the PEMFC with a fully hydrated PEM. After saturating the MEA with water, ^{1}H NMR microscopy images of the operating PEMFC show that the in-plane distribution of water in the Nafion remains uniform for a period of time (on the order of hours) regardless of gas flow configuration. Alternating the fuel supply between H_2(g) and D_2(g) introduced contrast that enabled investigation of changes in the water in the PEM when the PEMFC operated under steady-state conditions.

The ^{1}H NMR microscopy images and the integrated ^{1}H NMR signal intensities show that when the PEM is saturated with D_2O(l), H–D exchange with water in the PEM begins immediately upon operating the PEMFC with H_2(g) as fuel. For the H_2(g)/D_2(g) experiments, in contrast to the H_2(g)/D_2O(l) experiments, there was a significant delay in time prior to measurable H–D exchange with water in the PEM. These results are consistent with what is expected based on AFM studies that show an increase in the size of the conductive hydrophilic domains of Nafion in high relative humidity environments or those in contact with liquid water. As the currents were similar for these experiments, the results indicate that the current per area of conductive hydrophilic domain is higher when the PEM operates under low relative humidities. In addition, the integrated ^{1}H NMR signal intensities indicate that the period of time required for H–D exchange to be evident with water in the PEM is longer when operating on H_2(g) (D_2O hydrated PEM) versus D_2(g) (H_2O hydrated PEM), consistent with expected isotope effects.

In summary, the results presented demonstrate that H–D exchange is effective for introducing contrast in ^{1}H NMR microscopy images of operating PEMFCs. In addition, information can be garnered regarding the in situ distribution of water in the PEM between the operating catalyst layers and the utilization of the conductive hydrophilic domains of the PEM, information that is not available from other fuel cell diagnostic techniques.

Acknowledgements

Members of the solid-state NMR research group at the University of Alberta are thanked for helpful comments and discussions. Dr. Guy Bernard is thanked for aid with preparation of the manuscript. Dr. Thomas Oerther at Bruker-Biospin GmbH is thanked for technical support. Our PEMFCs are designed in conjunction with, and machined by, Dieter Starke in the Department of Chemistry machine shop. We appreciate the assistance of the Department of Chemistry electronics shop. Prof. Dr. Emil Roduner at the Universität Stuttgart is thanked for graciously providing us with a preprint of their recent AFM results. K.W.F. thanks the Natural Sciences and Engineering Research Council of Canada, NSERC, the Alberta Ingenuity Fund, and the University of Alberta for postgraduate scholarships. This research was funded by NSERC, the Canada Foundation for Innovation, Alberta Ingenuity, and the University of Alberta. R.E.W. thanks the Government of Canada for a Canada Research Chair in Physical Chemistry.

References

[1] J. Larminie, A. Dicks, Fuel Cell Systems Explained, 2nd ed., John Wiley and Sons Ltd., Chichester, 2003, pp. 75–90.
[2] M. Eikerling, A.A. Kornyshev, A.R. Kucernak, Phys. Today 59 (2006) 38–44.
[3] C.K. Dyer, Sci. Am. 281 (1999) 88–93.
[4] A.J. Appleby, Sci. Am. 281 (1999) 74–79.
[5] A.C. Lloyd, Sci. Am. 281 (1999) 80–84, 86.
[6] F. Barbir, PEM Fuel Cells: Theory and Practice, Elsevier Academic Press, San Diego, 2005, pp. 147–206.
[7] F. Barbir, PEM Fuel Cells: Theory and Practice, Elsevier Academic Press, San Diego, 2005, pp. 271–336.
[8] V. Mehta, J.S. Cooper, J. Power Sources 114 (2003) 32–53.
[9] F. Barbir, PEM Fuel Cells: Theory and Practice, Elsevier Academic Press, San Diego, 2005, pp. 115–145.
[10] R.C.T. Slade, J. Barker, J.H. Strange, Solid State Ionics 35 (1989) 11–15.

[11] T.A. Zawodzinski Jr., C. Derouin, S. Radzinski, R.J. Sherman, V.T. Smith, T.E. Springer, S. Gottesfeld, J. Electrochem. Soc. 140 (1993) 1041–1047.
[12] J.J. Fontanella, C.A. Edmondson, M.C. Wintersgill, Y. Wu, S.G. Greenbaum, Macromolecules 29 (1996) 4944–4951.
[13] M. Cappadonia, J.W. Erning, S.M.S. Niaki, U. Stimming, Solid State Ionics 77 (1995) 65–69.
[14] J. St-Pierre, D.P. Wilkinson, S. Knights, M.L. Bos, J. New Mater. Electrochem. Syst. 3 (2000) 99–106.
[15] K.A. Mauritz, R.B. Moore, Chem. Rev. 104 (2004) 4535–4585.
[16] R.J. Bellows, M.Y. Lin, M. Arif, A.K. Thompson, D. Jacobson, J. Electrochem. Soc. 146 (1999) 1099–1103.
[17] A.B. Geiger, A. Tsukada, E. Lehmann, P. Vontobel, A. Wokaun, G.G. Scherer, Fuel Cells 2 (2002) 92–98.
[18] K.W. Feindel, L.P.A. LaRocque, D. Starke, S.H. Bergens, R.E. Wasylishen, J. Am. Chem. Soc. 126 (2004) 11436–11437.
[19] S. Tsushima, K. Teranishi, S. Hirai, Electrochem. Solid-State Lett. 7 (2004) A269–A272.
[20] K.R. Minard, V.V. Viswanathan, P.D. Majors, L.-Q. Wang, P.C. Rieke, J. Power Sources 161 (2006) 856–863.
[21] K. Tüber, D. Pocza, C. Hebling, J. Power Sources 124 (2003) 403–414.
[22] J.P. Owejan, T.A. Trabold, D.L. Jacobson, D.R. Baker, D.S. Hussey, M. Arif, Int. J. Heat Mass Transfer 49 (2006) 4721–4731.
[23] T.A. Trabold, J.P. Owejan, D.L. Jacobson, M. Arif, P.R. Huffman, Int. J. Heat Mass Transfer 49 (2006) 4712–4720.
[24] A. Turhan, K. Heller, J.S. Brenizer, M.M. Mench, J. Power Sources 160 (2006) 1195–1203.
[25] D.J. Ludlow, C.M. Calebrese, S.H. Yu, C.S. Dannehy, D.L. Jacobson, D.S. Hussey, M. Arif, M.K. Jensen, G.A. Eisman, J. Power Sources 162 (2006) 271–278.
[26] K.W. Feindel, S.H. Bergens, R.E. Wasylishen, ChemPhysChem 7 (2006) 67–75.
[27] K.W. Feindel, S.H. Bergens, R.E. Wasylishen, J. Am. Chem. Soc. 128 (2006) 14192–14199.
[28] K.W. Feindel, S.H. Bergens, R.E. Wasylishen, Phys. Chem. Chem. Phys. 9 (2007) 1850–1857.
[29] A. Connelly, J.A.B. Lohman, B.C. Loughman, H. Quiquampoix, R.G. Ratcliffe, J. Exp. Bot. 38 (1987) 1713–1723.
[30] K. Ilvonen, L. Palva, M. Perämäki, R. Joensuu, R. Sepponen, J. Magn. Reson. 149 (2001) 36–44.
[31] J. Kawamura, K. Hattori, T. Hongo, R. Asayama, N. Kuwata, T. Hattori, J. Mizusaki, Solid State Ionics 176 (2005) 2451–2456.
[32] A. Loewenstein, A. Szöke, J. Am. Chem. Soc. 84 (1962) 1151–1154.
[33] S. Meiboom, J. Chem. Phys. 34 (1961) 375–388.
[34] D.X. Cao, S.H. Bergens, Electrochim. Acta 48 (2003) 4021–4031.
[35] P.T. Callaghan, Principles of Nuclear Magnetic Resonance Microscopy, Oxford University Press, New York, 1991.
[36] B. MacMillan, A.R. Sharp, R.L. Armstrong, Polymer 40 (1999) 2471–2480.
[37] J.A. Glasel, in: F. Franks (Ed.), Water: A Comprehensive Treatise, vol. 1, Plenum Press, New York, 1972.
[38] J.T. Hinatsu, M. Mizuhata, H. Takenaka, J. Electrochem. Soc. 141 (1994) 1493–1498.
[39] G. Gebel, P. Aldebert, M. Pineri, Polymer 34 (1993) 333–339.
[40] P.J. James, J.A. Elliott, T.J. McMaster, J.M. Newton, A.M.S. Elliott, S. Hanna, M.J. Miles, J. Mater. Sci. 35 (2000) 5111–5119.
[41] R.S. McLean, M. Doyle, B.B. Sauer, Macromolecules 33 (2000) 6541–6550.
[42] B. Halle, G. Karlström, J. Chem. Soc., Faraday Trans. 2 (79) (1983) 1031–1046.
[43] S.J. Sondheimer, N.J. Bunce, M.E. Lemke, C.A. Fyfe, Macromolecules 19 (1986) 339–343.
[44] V.M. Barragán, C. Ruíz-Bauzá, J.P.G. Villaluenga, B. Seoane, J. Colloid Interface Sci. 277 (2004) 176–183.
[45] T.A. Zawodzinski Jr., M. Neeman, L.O. Sillerud, S. Gottesfeld, J. Phys. Chem. 95 (1991) 6040–6044.
[46] K.R. Harris, L.A. Woolf, J. Chem. Soc., Faraday Trans. 1 (76) (1980) 377–385.
[47] R. Mills, J. Phys. Chem. 77 (1973) 685–688.
[48] H. Weingärtner, Z. Phys. Chem. 132 (1982) 129–149.
[49] J. Crank, The Mathematics of Diffusion, Clarendon Press, Oxford, 1956.
[50] F. Barbir, PEM Fuel Cells: Theory and Practice, Elsevier Academic Press, San Diego, 2005, pp. 33–72.
[51] M.N. Tsampas, A. Pikos, S. Brosda, A. Katsaounis, C.G. Vayenas, Electrochim. Acta 51 (2006) 2743–2755.
[52] A. Katsaounis, S. Balomenou, D. Tsiplakides, S. Brosda, S. Neophytides, C.G. Vayenas, Appl. Catal. B: Environ. 56 (2005) 251–258.
[53] P. Schroeder, Z. Phys. Chem. 45 (1903) 57.
[54] T.A. Zawodzinski, S. Gottesfeld, S. Shoichet, T.J. McCarthy, J. Appl. Electrochem. 23 (1993) 86–88.
[55] E. Aleksandrova, R. Hiesgen, D. Eberhard, K.A. Friedrich, T. Kaz, E. Rodner, ChemPhysChem 8 (2007) 519–522.